

Granular superconductivity in a Ca-doped $\text{YBa}_2\text{Cu}_3\text{O}_{7-\delta}$ single crystal: Role of divalent impurities and the effect of applied fields on the grain coupling

V. N. Vieira

Instituto de Física e Matemática, Universidade Federal de Pelotas, Caixa Postal 354, CEP 96010-900, Pelotas, Rio Grande do Sul, Brazil

I. C. Riegel

Instituto de Ciências Exatas e Tecnológicas, Centro Universitário Feevale, Campus II, RS 239, 2755, CEP 93352-000 Novo Hamburgo, Rio Grande do Sul, Brazil

J. Schaf*

Instituto de Física, Universidade Federal do Rio Grande do Sul (UFRGS), CEP 91501-970, Porto Alegre, Rio Grande do Sul, Brazil

(Received 9 February 2007; published 26 July 2007)

We investigate the effect of the divalent Ca atoms at the trivalent Y site of $\text{YBa}_2\text{Cu}_3\text{O}_{7-\delta}$ on the magnetoresistivity and magnetic irreversibility of single crystals and a polycrystalline sample. The magnetic irreversibility displays the de Almeida–Thouless and Gabay–Toulouse power laws, the signature of a frustrated superconducting grain aggregate for the $H\parallel c$ axis as well as for the $H\parallel ab$ plane. The resistive transition for measuring current along the ab plane and $H\parallel c$ axis is a clear two step process. While the upper temperature step is only weakly affected by applied fields, the lower temperature transition is visibly broadened and shifted down to lower temperatures. We impute the upper temperature step to the pairing transition within grains while the lower temperature step is due to grain coupling and coherence transition. For the $J\parallel ab$ and $H\parallel ab$ planes, the resistive transition is a one step process and the effect of the applied fields is very weak for $H\parallel J$ as well as for $H\perp J$. We explain these observations in terms of the directional anisotropy of the phase displacements between the superconducting grains and their weakening effect on the grain coupling, caused by the applied field. We also compare our present results with those of $\text{YBa}_2\text{Cu}_3\text{O}_{7-\delta}$ single crystals doped with the trivalent Pr at the Y site and with divalent elements such as Zn or Mg at the Cu site and Sr at the Ba site and suggest that the valence as well as the local breaking of the orbital symmetry by impurities plays an important role in the induction of superconducting granularity.

DOI: [10.1103/PhysRevB.76.024518](https://doi.org/10.1103/PhysRevB.76.024518)

PACS number(s): 74.81.-g, 74.81.Bd, 74.25.Qt

I. INTRODUCTION

Very clean and well oxygenated $\text{YBa}_2\text{Cu}_3\text{O}_{7-\delta}$ single crystals are homogeneous superconductors. However, all the less perfect single crystals show the features of superconducting granularity. Considering the very short coherence length of the superconducting order parameter of the high temperature superconducting cuprates (HTSCs), the features of superconducting granularity in polycrystalline samples are expected. Even the effect of impurities on the grain-boundary potential, band bending, and the corresponding electron phase shifts and their influence on the supercurrent through the grain boundaries seem well understood.^{1–3} However, explaining the features of superconducting granularity in single crystals is a challenging issue because single crystals are structurally fairly continuous systems. Even more defying is the fact that single crystals often develop two superconducting phases with two close and well-defined transition temperatures. Despite such a superconducting inhomogeneity is certainly due to some kind of chemical inhomogeneity, it seems difficult to ascertain which one.

The origin of superconducting granularity in doped $\text{YBa}_2\text{Cu}_3\text{O}_{7-\delta}$ single crystals has often been ascribed simply to the inhomogeneous distribution of impurity atoms. Presently, the effect of a number of different impurity atoms, located at the different lattice sites of $\text{YBa}_2\text{Cu}_3\text{O}_{7-\delta}$ is

known. The data, however, do not seem to indicate that the distribution of the impurities in the crystal lattice alone is determinant in causing superconducting granularity. Moreover, superconducting granularity often is displayed by pure $\text{YBa}_2\text{Cu}_3\text{O}_{7-\delta}$ single crystals.^{4,5} Some results provide indications that specific attributes of the impurity atoms such as valence, orbital symmetry, or ion size play an important role in the induction of superconducting granularity.^{6–9} The simple presence of impurities in the crystal lattice certainly introduces electronic inhomogeneity and lattice distortions, but it also favors an inhomogeneous oxygen distribution leading to superconducting inhomogeneity.

With the aim of obtaining information about the origin of superconducting granularity, caused by impurities at the Y site of $\text{YBa}_2\text{Cu}_3\text{O}_{7-\delta}$ single crystals as well as about the role of the valence and the orbital symmetry of the impurity atoms in the induction of superconducting granularity, we investigate the effect of divalent Ca ($4s^2$) at the trivalent Y ($4d^15s^2$) of $\text{YBa}_2\text{Cu}_3\text{O}_{7-\delta}$ single crystals on the magnetic irreversibility and magnetoresistance. We also contrast the present results with those of the trivalent Pr at the same Y site⁶ and compare these results with those for divalent Zn and Mg at the Cu site⁷ and those of Sr at the Ba site.^{8,9} All these impurities have been verified to favor superconducting granularity of $\text{YBa}_2\text{Cu}_3\text{O}_{7-\delta}$ single crystals.

Crystallographic and structural studies of the $Y_{1-x}Ca_xBa_2Cu_3O_{7-\delta}$ compound have shown that up to about 15 at. % ($x=0.15$) Ca substitutes only Y atoms.¹⁰⁻¹⁴ Beyond 15 at. %, some Ca goes to the Ba site. Although Ca doping causes no significant changes in the lattice parameters,¹⁰⁻¹⁴ the superconducting transition temperature decreases systematically with the Ca concentration. This shows that Ca doping increases the effective charge carrier density in the bulk, distorting the conductive CuO_2 layers.¹⁻³ However, favorably Ca doping also reduces the width and height of the potential barrier in the grain boundaries between neighboring grains, thereby improving grain connection and the overall critical current of a grain aggregate.¹⁻³ Moreover, Ca doping has also been observed to favor superconductivity in oxygen deficient materials.¹²

Several studies with specific techniques such as thermoelectric power,¹⁰ magnetization^{10,15} electric transport,^{10,11,13,16-19} magnetic irreversibility,¹⁷ and capacitance²⁰ have provided information on the effect of Ca on the electric and superconducting properties of polycrystalline samples of the $Y_{1-x}Ca_xBa_2Cu_3O_{7-\delta}$ compound. Recently a micro-Raman study of fully oxygenated $Y_{1-x}Ca_xBa_2Cu_3O_{7-\delta}$ ceramic samples has evidenced a phase separation into an optimally doped and an overdoped phase, this last with a slightly lower transition temperature.²¹ This phase separation may elucidate the occurrence of the two close genuine superconducting transitions often observed in cuprates.^{6,22,23} Although considerable progress has been made in the polycrystalline $Y_{1-x}Ca_xBa_2Cu_3O_{7-\delta}$ materials, only very few attempts have succeeded in growing $Y_{1-x}Ca_xBa_2Cu_3O_{7-\delta}$ single crystals.²⁴⁻²⁶ Moreover, sample analysis showed that the single crystals, grown by the self-flux method, contain a Ca concentration much lower than the nominal concentration.²⁵

II. SAMPLE PREPARATION AND MEASURING TECHNIQUES

We have prepared a polycrystalline sample of the $Y_{0.95}Ca_{0.05}Ba_2Cu_3O_{7-\delta}$ compound and single crystals with about 2 at. % Ca at the Y site. The polycrystalline sample was prepared by the usual method of reaction in solid. The single crystals were grown by the standard self-flux method. The elemental proportion in the initial mix was 0.95:0.05:4:10 of, respectively, Y, Ca, Ba, and Cu with no other additives. For temperature cycle and oxygenation, treatment is the same as used in Ref. 7. X-ray diffraction made in one representative single crystal of the batch showed a very clean single phase orthorhombic structure, see Fig. 1. Examination of the single crystals by polarized light microscopy showed densely twinned domains. Some were almost twinning monodomains, others showed complex landscapes of orthogonal domains. Examination by scanning electron microscopy (SEM) showed in several single crystals interrupted cracks, but some crystals showed stripes like that on top of Fig. 1, which we think are healed cracks. Energy dispersive spectroscopy spectra confirmed the presence of Ca in the single crystals.

The magnetoresistance measurements were made by the four contacts, low-current-low-frequency ac null technique

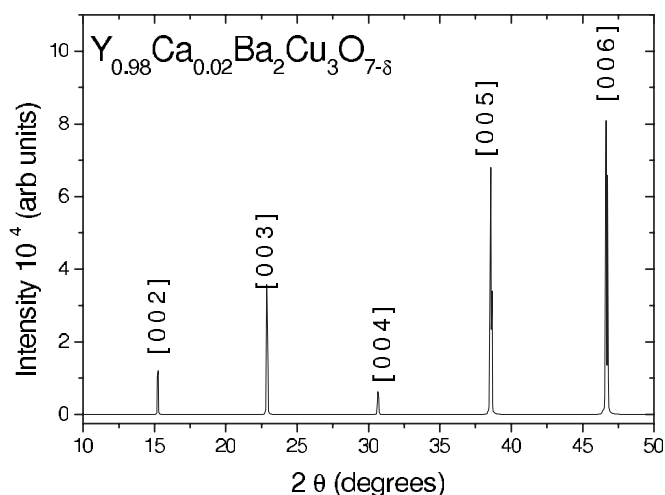


FIG. 1. The upper panel displays the SEM image of the twin of SCr1. Remark the strip across it. The spots are residues of flux. The lower panel shows the very clean x-ray diffraction pattern of a single crystal of the same batch for incidence along the c axis.

in constant applied fields up to 0.5 kOe. During the measurements, the temperature was swept (down) very slowly (0.05 K/min) and measured with a Pt thermometer, corrected for magnetoresistance effects within a resolution of 2×10^{-3} K. The magnetoresistance data points measured are spaced closely enough to numerically calculate the temperature derivative of the resistivity, dp/dT .

The magnetic irreversibility was obtained from dc magnetization measurements using a SQUID-MPMS-XL magnetometer from Quantum Design. The method consisted in first cooling down the sample to temperatures well below T_c in zero field (ZFC), then measuring the magnetization (M_{ZFC}) while slowly warming (0.2 K/min or less) up to $T \gg T_c$ under applied fields within the range from 0.003 to 50 kOe and subsequently measuring M_{FC} while cooling back (FC) in the same field.

III. EXPERIMENTAL RESULTS

A. Magnetic irreversibility

We have determined the magnetic irreversibility limits of the single crystal SCr1, the same used in the magnetoresistance measurements, and a polycrystalline sample by using

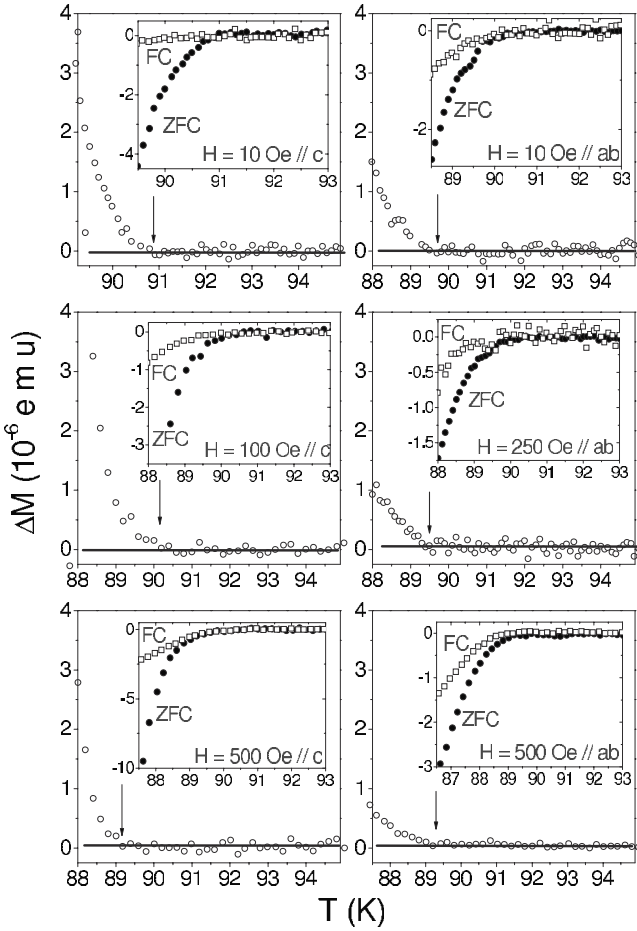


FIG. 2. Examples of the differences $M_{FC} - M_{ZFC}$ data (main figure) and the M_{ZFC} and M_{FC} magnetization data (inset) showing details of our data analysis. The vertical arrows indicate the irreversibility limits $T_{irr}(H)$.

the zero-field-cooled (M_{ZFC}) and field-cooled (M_{FC}) dc magnetization techniques as a function of temperature for a large number of applied magnetic fields up to 50 kOe. The single crystal has the form of a platelet of nearly rectangular shape about 1.5 mm in length, 0.5 mm in broadness, and 0.1 mm in thickness. This sample was broken up from a bigger single crystal, the counterpart of which is shown in the SEM image (top panel) of Fig. 1. This single crystal exhibits a strip across it, which seems to be a healed crack. The polycrystalline sample was of an elongated form aligned with the applied field to minimize the demagnetizing field. In our method, the irreversibility limit for a given applied field is the temperature point $T_{irr}(H)$ where the $\Delta M = M_{FC} - M_{ZFC}$ data leave the zero base line, defined by the high temperature region, where the magnetization of the sample is reversible. Figure 2 exemplifies and shows details of our data analysis, see also Ref. 7. The low field $T_{irr}(H)$ data of the single crystal SCr1 are plotted for the $H \parallel c$ axis and the $H \parallel ab$ plane in Fig. 3. While the main figure highlights the low field data, which are of special interest here, the inset displays the $T_{irr}(H)$ data of the single crystal for the $H \parallel c$ axis and of the polycrystalline sample in the whole field range. The continuous lines through the high field $T_{irr}(H)$ data are fittings with

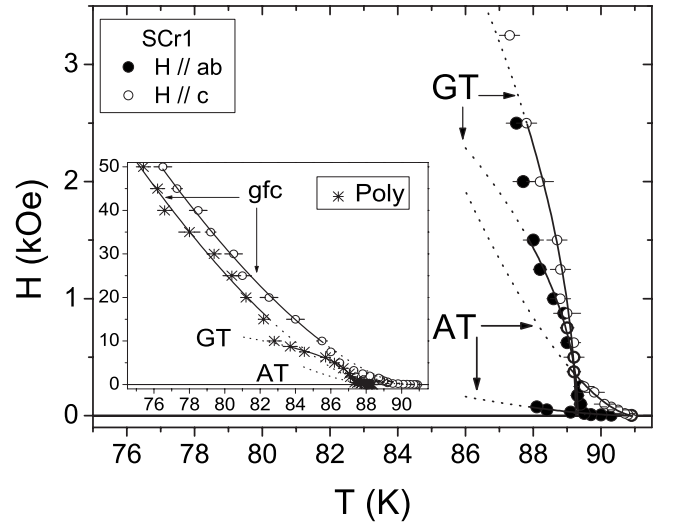


FIG. 3. The low field $T_{irr}(H)$ data of the SCr1 sample for the $H \parallel c$ axis and the $H \parallel ab$ plane. The continuous lines assigned by AT and GT are fittings to the de Almeida–Thouless and Gabay–Toulouse power laws, respectively. The inset shows the $T_{irr}(H)$ data of the SCr1 for the $H \parallel c$ axis and of the Poly sample in the whole field range. The continuous lines through the high field data assigned by gfc are fittings with Eq. (1). The AT and GT regimes in the low field region of the polycrystalline sample are already clear in the inset figure.

the power law, predicted for the irreversibility line by the giant-flux-creep theory:²⁷

$$H_{irr}(T) = H_0(1-t)^\alpha \quad \left(\alpha = \frac{3}{2} \right). \quad (1)$$

In Eq. (1), $t = T_{irr}(H)/T_{irr}(0)$ is the reduced temperature, and H_0 and $T_{irr}(0)$ are fitting parameters, which are, respectively, the irreversibility field at zero temperature and the extrapolation of $T_{irr}(H)$ to zero field. The continuous lines through the low field data in the main figure are fittings with the de Almeida–Thouless (AT)-like [$\alpha = 3/2$ in Eq. (1)] (Ref. 28) and the Gabay–Toulouse (GT)-like [$\alpha = 1/2$ in Eq. (1)] (Ref. 29) power laws. Although the AT and GT power laws proceed from mean field calculations for the frustrated Ising-like and three-dimensional XY spin-glass systems, respectively, they describe quite well the irreversibility lines of our superconductor samples. This is no surprise as the grain coupling of superconducting grain aggregates under applied magnetic field is well known to be dominated by frustration likewise spin coupling in spin-glass systems. Table I lists our fitting parameters H_0 and $T_{irr}(0)$ for, respectively, the giant-flux-creep (gfc), AT-, and GT-like power law regimes of our samples.

B. Magnetoresistive transition

Our sample is an $Y_{0.98}Ca_{0.02}Ba_2Cu_3O_{7-\delta}$ single crystal, the same used in the magnetic measurements, named SCr1. We obtained a high density of data points while slowly cooling the sample through the superconducting transition region

TABLE I. The gfc, AT, and GT power law exponents α , the parameters H_0 , and $T_{irr}(0)$ from fittings of the $T_{irr}(H)$ data of the SCr1 sample ($Y_{0.98}Ca_{0.02}Ba_2Cu_3O_{7-\delta}$) and the polycrystalline sample (Poly) to the flux creep, de Almeida–Thouless (AT), and the Gabay-Toulouse (GT) power laws.

Samples	Fit	α	H_0 (kOe)	$T_{irr}(0)$ (K)
SCr1 ($H\parallel c$)	gfc	1.49 ± 0.12	970.39	91.02
	GT	0.56 ± 0.14	19.84	90.73
	AT	1.60 ± 0.09	17.42	90.90
SCr1 ($H\parallel ab$)	GT	0.51 ± 0.09	12.18	89.32
	AT	1.60 ± 0.27	17.42	90.90
Poly	gfc	1.49 ± 0.22	870.56	90.20
	GT	0.42 ± 0.12	33.24	88.99
	AT	1.41 ± 0.15	582.02	90.20

under constant applied magnetic fields. The upper panels of Fig. 4 display the resistive transition of the Ca-doped single crystal, measured for low measuring current along the ab plane and for three directions of the applied field, as indicated in the figure. The overall trends of $\rho(T)$ are similar for all the current-field configurations, as is usual.^{7,9} However, there are also remarkable differences. For the $H\parallel c$ axis, the resistive transition moves markedly with increasing applied field toward the lower temperature side. Moreover, the resistivity falls in two main steps of similar sizes and finally, after a long and bumpy foot, it falls effectively to zero. Two step resistive transitions in single crystals in general characterize granular superconductivity. For fields applied along the ab plane and $H\parallel J$, the transition temperature is practically insensitive to the applied field and the two step resistive transition seems unique. For $H\parallel ab \perp J$, the effect of the applied field is also much weaker than for the $H\parallel c$ axis. However, for all the measuring configurations, the foot of the resistive transition, which we ascribe to minority phases, is very similar. These features are not a peculiarity of the single crystal depicted in Fig. 4 but have also been observed in two other single crystals of the same batch and not shown here.

The lower panels of Fig. 4 display the respective temperature derivatives $d\rho(T)/dT$. The $d\rho(T)/dT$ data for the $H\parallel c$ axis show very clearly that the main resistive transition falls in two stages. The upper temperature peak indicated by T_p is centered at 91 K for an applied field of 10 Oe. T_p is well known to correspond closely but not exactly to the pairing transition within the superconducting grains. Comparison of this peak temperature value with those of Ref. 25 shows that in our single crystal, about 2 at. % of the Y atoms are substituted by Ca. For increasing applied field, the T_p peak becomes somewhat broader and somewhat lower and moves a little bit toward lower temperatures. However, the lower temperature peak is much more sensitive to the applied field, which characterizes it as a grain coupling feature and a coherence transition. The temperature derivatives of the resistive transitions for the other current-field configurations are displayed in the central and right-hand panels of Fig. 4, re-

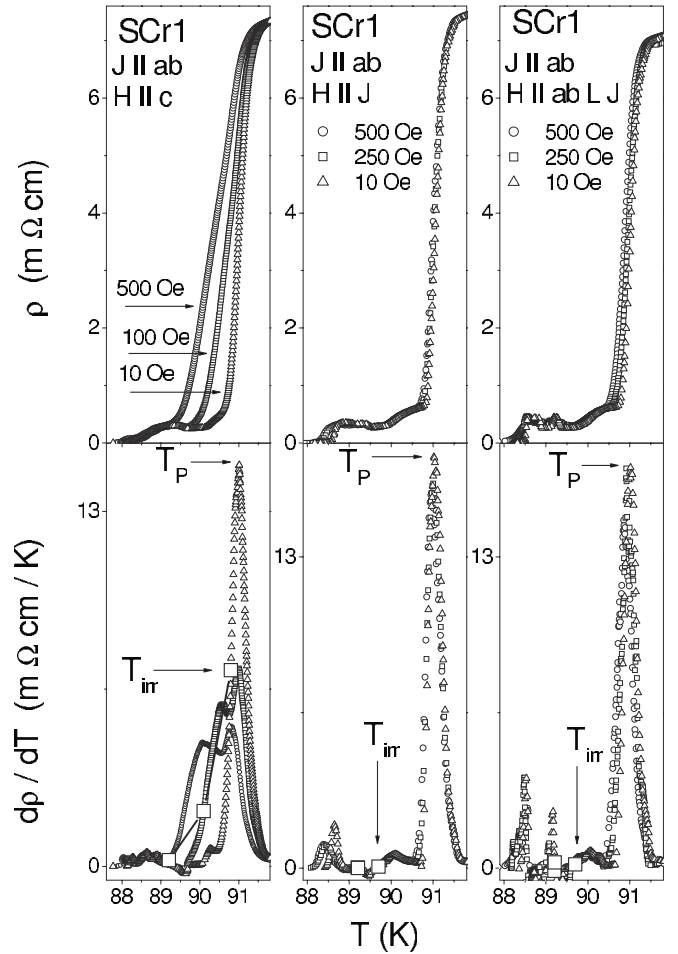


FIG. 4. The upper panels from left to right display the resistive transitions of the SCr1 for the indicated field values and the specified current-field configurations. The lower panels display the respective temperature derivatives.

spectively. In particular, $\rho(T)$ and $d\rho(T)/dT$ for the configuration, represented in the central panels, are almost completely insensitive to the applied field. The two step resistive transition apparently takes place in a unique step. For the configuration, represented in the right-hand panels, the effect of the field is also very low and the two step resistive transition is also imperceptible.

The open squares in the lower panels of Fig. 4 indicate the magnetic irreversibility limits for the corresponding applied fields. The fact that these limits occur halfway between the pairing transition and the coherence transition shows that the flux trapping by coupled grain loops only becomes relevant when the first coupled grain loops become stable. Zero resistance takes place only when grain coupling diverges and extends over the whole sample. In the case of our Ca-doped YBaCuO single crystal, this occurs close to 88 K, where the resistivity falls to zero.

We have also measured the resistive transition and the magnetic irreversibility of a polycrystalline $YBa_2Cu_3O_{7-\delta}$ sample doped with 5% Ca at the Y site. The resistive transition of this sample follows the usual trends of granular superconductors.^{30,31}

IV. DISCUSSION

Superconducting granularity becomes evident from magnetoresistance and magnetic irreversibility because of the fragility of the grain couplings to applied fields. In magnetoresistance, grain coupling gives rise to a field dependent coherence transition while in the magnetic irreversibility, it manifests by the presence of the AT and GT power law regimes in the low field region, which are the signature of frustrated systems. Frustration in granular superconductors arises due to the multiconnectedness of the superconducting grains and the phase disorder introduced by the applied field leading to conflicting couplings and the impossibility of minimizing the coupling energy. Frustration, magnetic irreversibility, and magnetoresistance in granular superconductors are thus intimately connected. These facts have been used often to test for superconducting granularity of superconducting materials.^{7-9,30,31} In single crystals with a granular superconducting character, the grain junctions in general are more uniform and therefore the coherence transition is much narrower and the low field range where the magnetic irreversibility displays the AT and GT regimes is smaller than in polycrystalline materials.^{8,31}

The superconducting granularity of our $Y_{0.98}Ca_{0.02}Ba_2Cu_3O_{7-\delta}$ single crystal is well characterized by the presence of the AT and GT power law regimes in the low field magnetic irreversibility as well as by the clear coherence transition in the resistive transition. However, the feature of this coherence transition as well as the region of the AT and GT regimes in the magnetic irreversibility is much more important than in previously measured doped $YBa_2Cu_3O_{7-\delta}$ single crystals with a granular superconducting character.^{7,9,30}

Besides the features of superconducting granularity, the magnetoresistance data of our $Y_{0.98}Ca_{0.02}Ba_2Cu_3O_{7-\delta}$ single crystal for the different current-field configurations reveal other very interesting features. They display with an unprecedented clearness the nature of the physical mechanism by which the applied magnetic field affects the grain coupling and resistivity. Weakly coupled superconducting grain aggregates under an applied field are usually described in terms of the effective Josephson coupling Hamiltonian:³²

$$H = - \sum_{i,j} J_{ij} \cos(\theta_i - \theta_j - A_{ij}). \quad (2)$$

Here, J_{ij} are the phase coupling energies between neighboring grains i and j and $\theta_i - \theta_j$ is the phase difference of the Ginzburg-Landau (GL) order parameter on the grains i and j . The phase displacements A_{ij} are given by

$$A_{ij} = \frac{2\pi}{\phi_0} \int_i^j \vec{A} \cdot d\vec{l}, \quad (3)$$

where ϕ_0 is the elementary flux quantum, \vec{A} is the vector potential along the weak links between grains i and j , and the line integral is evaluated between the centers of grains i and j . Equation (3) asserts that an applied field causes phase displacements of the GL order parameter only along weak links that have a component along the vector potential, that is, extend transversely to the applied field and hence weak

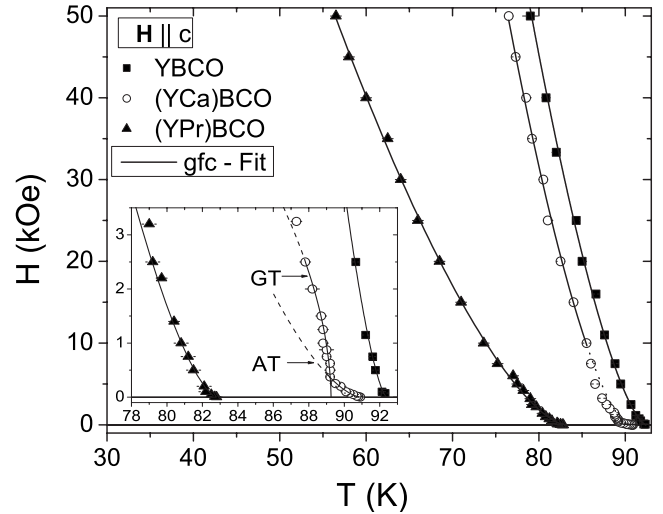


FIG. 5. From left to right, the $T_{irr}(H)$ data of $Y_{0.85}Pr_{0.15}Ba_2Cu_3O_{7-\delta}$ single crystal [(YPr)BCO], the single crystal SCr1 [(YCa)BCO], and of a highly pure $YBa_2Cu_3O_{7-\delta}$ single crystal (YBCO). The continuous lines through the data are fittings with Eq. (1). The inset highlights the low field data, where the continuous lines, assigned AT and GT on the data of SCr1, are fittings with, respectively, the de Almeida-Thouless- and the Gabay-Toulouse-like power laws. Note that only the Ca-doped single crystal displays the signatures of superconducting granularity. The other data comply with the gfc fit in the whole region.

links directed along the field are not affected. Phase disorder weakens grain coupling, favors the phase fluctuations, and consequently lowers the electric conductivity and the flux stabilizing capability. This effect, however, depends strongly on the current-field configuration, as shown by Eq. (3). In the particular case of the left-hand panels of Fig. 4, the applied field is along the c axis and the measuring current is perpendicular to the applied field. Therefore, the vector potential runs within the ab plane about the applied field direction and hence its component along the lateral weak links, along which the measuring current flows, is large and the phase displacements A_{ij} in Eq. (2) are large. In the case of the central panel of Fig. 4, the field is applied along the ab plane, parallel to the measuring current, so that the vector potential is throughout perpendicular to the weak links transporting the measuring current and hence the phase displacements A_{ij} vanish. This will say that the effect of the field on the relevant grain couplings is minimized. Finally, the right-hand panels of Fig. 4 show the resistive transition for field along the ab plane but normal to the current. In that case, the effect of the field is small because the sample thickness is very much smaller than its broadness and therefore the component of the vector potential along the weak links transporting the measuring current is very much lower than for the field along the c axis. Dissipation by flux activation is also much smaller due to the intrinsic flux pinning.

We may also compare our present results with those of the same compound doped with other impurities. A large number of examples of doped $YBa_2Cu_3O_{7-\delta}$ single crystals with a granular superconducting character can be found in Refs. 7, 9, and 30. The $T_{irr}(H)$ data in all these cases exhibit, in the

major high field range, the power law of the gfc regime. In only very few exceptions like the Pr doped⁶ and a well oxygenated pure $\text{YBa}_2\text{Cu}_3\text{O}_{7-\delta}$ single crystal³⁰ for which the $T_{irr}(H)$ data follow the gfc regime in the whole field range, all the other studied pure or doped $\text{YBa}_2\text{Cu}_3\text{O}_{7-\delta}$ single crystals exhibit in a low field range the AT and GT regimes, the signature of frustration. In order to show this, we display in Fig. 5 the $T_{irr}(H)$ data of these samples together with those of the present Ca-doped single crystal. The figure displays only the data for the $H\parallel c$ axis because the features for the $H\parallel ab$ plane are entirely analogous. The Pr-doped single crystal, in fact, is a very curious example. The resistive transition of this compound exhibits two very close and genuine superconducting transitions, which forcibly implies superconducting granularity. Nevertheless, the single crystal does not display the features of frustration nor does it show a coherence transition in the resistive transition. In order to explain this unusual behavior, the authors assumed that, despite superconducting grains present, they remain isolated and therefore do not display a coherence transition or the characteristics of frustration.⁶

The fact that Ca at the Y site causes strong symptoms of superconducting granularity while Pr at the same site does not is very significant. Apparently, the different valences of Ca and Pr play a major role. Nevertheless, if the valence of the impurity were so decisive, then the effect of 1 at. % Zn or Mg at the Cu site, which have equal valences, would have to be very mild. Contrarily, Zn and Mg are well known to very drastically affect the superconductivity of $\text{YBa}_2\text{Cu}_3\text{O}_{7-\delta}$ and to lead to superconducting granularity.⁷ These facts indicate that another vigorous factor is playing there. The superconducting state of the HTSC is well known to be largely dominated by the $d_{(x^2-y^2)}$ orbital symmetry.^{33,34} Apparently,

breaking of this orbital symmetry by impurity atoms very drastically affects the superconducting state.³⁵ We guess that the different orbital symmetries of the impurity atoms play an important role in the patterning of the superconducting granularity. The electronic configuration and orbital symmetry of Ca ($4s^2$) differ considerably from that of Pr ($4f^36s^2$) and Y ($4d^15s^2$).

The effect of Sr at the Ba site of $\text{YBa}_2\text{Cu}_3\text{O}_{7-\delta}$ is rather moderate, but substitution of large proportions of Ba by Sr also leads to superconducting granularity.^{7-9,30} The perturbation of Sr takes place not via orbital symmetry breaking but via lattice distortion. The ionic radius of Sr is considerably smaller than that of Ba. Crystallographic studies have shown that Sr locally pulls together the neighboring couples of the CuO_2 planes, thereby introducing extensive distortion in the planar superconducting morphology.

In summary, we have prepared good $\text{Y}_{0.98}\text{Ca}_{0.02}\text{Ba}_2\text{Cu}_3\text{O}_{7-\delta}$ single crystals and determined their superconducting morphology from magnetoresistance and magnetic irreversibility data. Both techniques consistently show that these single crystals are granular superconductors. Our magnetoresistance data for the different current-field configurations also display very clearly the physical mechanism by which the applied magnetic field affects the superconducting grain coupling and the coherence transition. On the other hand, our results show that granular superconductivity can be induced in the $\text{YBa}_2\text{Cu}_3\text{O}_{7-\delta}$ system by impurities in whatever site Y, Ba, or Cu.

ACKNOWLEDGMENTS

The authors thank the Brazilian agencies CNPq and FAPERGS for partially financing this work.

*Corresponding author. FAX: (55) (51) 3308 7286; schaf@if.ufrgs.br

¹M. A. Schofield, M. Beleggia, Y. Zhu, K. Guth, and C. Jooss, Phys. Rev. Lett. **92**, 195502 (2004).

²G. Hammerl, A. Schmehl, R. R. Schulz, B. Goetz, H. Bielefeldt, C. W. Schneider, H. Hilgenkamp, and J. Mannhart, Nature (London) **407**, 162 (2000).

³J. Mannhart and H. Hilgenkamp, Mater. Sci. Eng., B **56**, 77 (1998).

⁴M. Daeumling, J. M. Seuntjens, and D. C. Larbalestier, Nature (London) **346**, 332 (1990).

⁵L. Krusin-Elbaum, L. Civale, F. Holtzberg, A. P. Malozemoff, and C. Feild, Phys. Rev. Lett. **67**, 3156 (1991).

⁶F. M. Barros, P. Pureur, J. Schaf, F. W. Fabris, V. N. Vieira, A. R. Jurelo, and M. P. Cantao, Phys. Rev. B **73**, 094515 (2006).

⁷V. N. Vieira, P. Pureur, and J. Schaf, Phys. Rev. B **66**, 224506 (2002).

⁸V. N. Vieira, P. Pureur, and J. Schaf, Physica C **353**, 241 (2001).

⁹V. N. Vieira and J. Schaf, Phys. Rev. B **65**, 144531 (2002).

¹⁰B. Fisher, J. Genossar, C. G. Kuper, L. Patlagan, G. M. Reisner, and A. Knizhnik, Phys. Rev. B **47**, 6054 (1993).

¹¹V. P. S. Awana and A. V. Narlikar, Phys. Rev. B **49**, 6353 (1994).

¹²V. P. S. Awana, Ashwin Tulapurkar, S. K. Malik, and A. V. Narlikar, Phys. Rev. B **50**, 594 (1994).

¹³S. K. Bandyopadhyay *et al.*, Phys. Lett. A **226**, 237 (1997).

¹⁴A. P. B. Sinha, K. K. Singh, and D. E. Morris, Physica C **266**, 44 (1966).

¹⁵A. Lascialfari, A. Rigamonti, L. Romano, P. Tedesco, A. Varlamov, and D. Embriaco, Phys. Rev. B **65**, 144523 (2002).

¹⁶A. K. Ghosh, S. K. Bandyopadhyay, P. Barat, Pintu Sen, and A. N. Basu, Physica C **264**, 255 (1996).

¹⁷A. Augieri, T. Petrisor, G. Celentano, L. Ciontea, V. Galluzzi, U. Gambardella, A. Mancini, and A. Ruffoloni, Physica C **401**, 320 (2004).

¹⁸J. T. Kucera and J. C. Bravman, Phys. Rev. B **51**, 8582 (1995).

¹⁹Y. Sun, G. Strasser, E. Gornik, and X. Z. Wang, Physica C **223**, 14 (1994).

²⁰J. H. T. Ransley *et al.*, Phys. Rev. B **70**, 104502 (2004).

²¹E. Liarokapis, D. Palles, D. Lampakis, G. Bottger, K. Conder, and E. Kaldis, Phys. Rev. B **71**, 014303 (2005).

²²V. N. Vieira, P. Pureur, and J. Schaf, Physica C **354**, 299 (2001).

²³R. Menegotto Costa, A. R. Jurelo, P. Rodrigues, Jr., P. Pureur, J. Schaf, J. V. Kunzler, L. Ghivelder, J. A. Campá, and I. Rasines, Physica C **251**, 175 (1995).

- ²⁴G. Botger, H. Schwer, E. Kaldis, and K. Bente, *Physica C* **275**, 198 (1997).
- ²⁵C. Chen, F. Wondre, A. J. S. Chowdhury, J. W. Hobby, and J. F. Ryan, *Physica C* **341-348**, 589 (2000).
- ²⁶K. C. Hewitt, X. K. Chen, C. Roch, J. Chrzanowski, J. C. Irwin, E. H. Altendorf, R. Liang, D. Bonn, and W. N. Hardy, *Phys. Rev. B* **69**, 064514 (2004).
- ²⁷Y. Yeshurun and A. P. Malozemoff, *Phys. Rev. Lett.* **60**, 2202 (1988).
- ²⁸J. R. L. de Almeida and D. J. Thouless, *J. Phys. A* **11**, 983 (1978).
- ²⁹M. Gabay and G. Toulouse, *Phys. Rev. Lett.* **47**, 201 (1981).
- ³⁰V. N. Vieira, J. P. da Silva, and J. Schaf, *Phys. Rev. B* **64**, 094516 (2001).
- ³¹J. Roa-Rojas, R. Menegotto Costa, P. Pureur, and P. Prieto, *Phys. Rev. B* **61**, 12457 (2000).
- ³²W. Y. Shih, C. Ebner, and D. Stroud, *Phys. Rev. B* **30**, 134 (1984).
- ³³C. C. Tsuei and J. R. Kirtley, *Rev. Mod. Phys.* **72**, 969 (2000).
- ³⁴C. C. Tsuei, J. R. Kirtley, G. Hammerl, J. Mannhart, H. Raffy, and Z. Z. Li, *Phys. Rev. Lett.* **93**, 187004 (2004).
- ³⁵N. C. Yeh *et al.*, *Phys. Rev. Lett.* **87**, 087003 (2001).